

# Two dimensional numerical experiments of atmospheric convection with condensation of the major component

Tatsuya Yamashita\*, Masatsugu Odaka\*, Ko-ichiro Sugiyama\*, Kensuke Nakajima\*\*, Masaki Ishiwatari\*, Yoshi-Yuki Hayashi†

\* Department of CosmoSciences, Graduate School of Science, Hokkaido University

\*\* Department of Earth and Planetary Sciences, Faculty of Sciences, Kyushu University

† Department of Earth and Planetary Sciences, Graduate School of Science, Kobe University

## 1 Introduction

In Martian atmosphere, atmospheric major component, CO<sub>2</sub>, condenses. CO<sub>2</sub> ice clouds are formed in current Martian polar regions (Pettengill and Ford, 2000). It is discussed that CO<sub>2</sub> ice clouds cause warm climate in early Mars (Forget and Pierrehumbert, 1997; Mitsuda, 2007). It is pointed out that supersaturation can influence significantly CO<sub>2</sub> cloud structure for convection with condensation of major component (Colaprete *et al.*, 2003). Laboratory experiments and observations suggest the emergence of super saturated regions in Martian atmosphere (Glandorf *et al.*, 2002).

Colaprete *et al.* (2003) discusses that high convective clouds which reach near tropopause does not develop but only thin clouds emerges the condensation level for the case that supersaturation is inhibited. In this case, temperature of ascent region must be equal to that of descent region, and air parcel can not obtain buoyancy due to degeneracy of degrees of freedom for thermodynamic variables. Colaprete *et al.* (2003) also shows that active cloud convection can occur if highly supersaturation is permitted in CO<sub>2</sub> atmosphere.

However, Colaprete *et al.* (2003) uses vertical one dimensional model in which convective motion is parameterized. Cloud convection model should be used in order to investigate cloud structure with condensation of major component, since cloud distribution is affected greatly by distribution of ascent and descent regions.

We have been developing cloud convection model in order to investigate atmospheric convective structure in various planets (e.g., Nakajima *et al.*, 2000; Odaka *et al.*, 2006; Sugiyama *et al.*, 2009). Odaka *et al.* (2006) incorporates the effects of condensation of major component into the cloud convection model, and perform

numerical experiments of ascending thermal plume as a test calculation. In this paper, we improve condensation process in the model of Odaka *et al.* (2006), and perform long time integration in order to investigate flow field and cloud distribution in statistical equilibrium states with considering supersaturation.

## 2 Model description

We assume that atmosphere consists entirely of CO<sub>2</sub>. The governing equations are the extension of quasi-compressible equations by Klemp and Wilhelmson (1978).

We extend quasi-compressible equations (Klemp and Wilhelmson, 1978) and use them as governing equations.

$$\frac{du}{dt} = -c_p \bar{\theta} \frac{\partial \pi}{\partial x} + D_m(u), \quad (1)$$

$$\frac{dw}{dt} = -c_p \bar{\theta} \frac{\partial \pi}{\partial z} + g \frac{\theta'}{\bar{\theta}} + D_m(w), \quad (2)$$

$$\begin{aligned} \frac{\partial \pi}{\partial t} + \frac{R\bar{\pi}}{c_v \bar{\rho} \bar{\theta}} \left[ \frac{\partial (\bar{\rho} \bar{\theta} u)}{\partial x} + \frac{\partial (\bar{\rho} \bar{\theta} w)}{\partial z} \right] \\ = \frac{R\bar{\pi}}{c_v \bar{\rho}} \left( \frac{L}{c_p \bar{T}} - 1 \right) \frac{M_c}{\bar{\rho}}, \end{aligned} \quad (3)$$

$$\begin{aligned} \frac{d\theta}{dt} + w \frac{\partial \bar{\theta}}{\partial z} = \frac{1}{\bar{\pi}} \left( \frac{LM_c}{\bar{\rho} c_p} + Q_{dis} + Q_{rad} \right) \\ + D_h(\theta), \end{aligned} \quad (4)$$

$$\begin{aligned} \frac{\partial \rho_s}{\partial t} + \frac{\partial (\rho_s u)}{\partial x} + \frac{\partial (\rho_s w)}{\partial z} \\ = M_c + D_h(\rho_s), \end{aligned} \quad (5)$$

where

$$\frac{d}{dt} = \frac{\partial}{\partial t} + u \frac{\partial}{\partial x} + w \frac{\partial}{\partial z}, \quad (6)$$

$$D_m(\cdot) = \frac{\partial}{\partial x} \left[ K_m \frac{\partial (\cdot)}{\partial x} \right] + \frac{1}{\bar{\rho}} \frac{\partial}{\partial z} \left[ \bar{\rho} K_m \frac{\partial (\cdot)}{\partial z} \right], \quad (7)$$

$$D_h(\cdot) = \frac{\partial}{\partial x} \left[ K_h \frac{\partial(\cdot)}{\partial x} \right] + \frac{1}{\bar{\rho}} \frac{\partial}{\partial z} \left[ \bar{\rho} K_h \frac{\partial(\cdot)}{\partial z} \right]. \quad (8)$$

$u, w$  are horizontal and vertical component of velocity, respectively.  $\pi$  is the Exner function,  $\theta$  is potential temperature, and  $T$  is temperature. Overbar denotes the basic state which depends only on height.  $K_m$  and  $K_h$  are eddy coefficients for momentum and heat, respectively.  $Q_{dis}$  is heating rate of dissipation.  $K_m, K_h$  and  $Q_{dis}$  are calculated by using 1.5 order closure (Klemp and Wilhelmson, 1978).  $Q_{rad}$  is heating rate of radiation,  $M_c$  is condensation rate, and  $L$  is latent heat of fusion.  $c_p, c_v$  are specific heat at constant pressure and volume, respectively.  $R$  is gas constant for unit mass, and  $g$  are gravitational acceleration.

We do not deal with radiation transfer explicitly, but we give horizontally uniform heating and cooling  $Q_{rad}$ . Heating and cooling rate is adjusted to retain heat balance of the entire system. Surface fluxes of momentum and heat are not considered in our model. Planetary rotation is not considered in our model.

Condensation of CO<sub>2</sub> occurs when saturation ratio  $S = p/p_*$  exceeds critical value  $S_{cr}$ , where  $p$  is pressure, and  $p_*$  is saturated vapor pressure.  $p_*$  is given by

$$p_* = \exp \left( A_{ant} - \frac{B_{ant}}{T} \right), \quad (9)$$

where  $A_{ant} = 27.4$  [Pa],  $B_{ant} = 3103$  [K] (The society of chemical engineers of Japan, 1999). If cloud particles grow by diffusion process, and growth by coalescence process can be neglected, condensation rate  $M_c$  are expressed as follows (Tobie et al., 2003).

$$M_c = \frac{4\pi r(S-1)N}{L^2/k_d RT} \quad \text{if} \quad \begin{cases} S > S_{cr} \\ S \leq 1, \rho_s \neq 0 \\ 1 < S \leq S_{cr}, \rho_s > \varepsilon \end{cases} \quad (10)$$

where  $r$  is cloud particle radius,  $N$  is number density of condensation nuclei, and  $k_d$  is heat conduction coefficient. We use the value of  $k_d = 4.8 \times 10^{-3}$  [W K<sup>-1</sup> m<sup>-1</sup>] (Tobie *et al.*, 2003).  $\varepsilon$  is a threshold constant for inhibiting unphysical condensation which can occur when saturation ratio is large. From (9) and Clausius-Clapeyron equation, latent heat  $L$  is constant value, then we obtain  $L = B_{ant}R$ .

If cloud particles radii  $r$  in one grid domain are constant,  $r$  is expressed by cloud density  $\rho_s$  and condensation nucleus radius  $r_d$ :

$$r = \left( r_d^3 + \frac{3\rho_s}{4\pi N\rho_I} \right)^{1/3}, \quad (11)$$

where  $\rho_I$  is the density of CO<sub>2</sub> ice, and we take  $\rho_I = 1.565 \times 10^3$  [kg/m<sup>3</sup>] (National Astronomical Observatory of Japan, 2004).  $r_d$  is 0.1 [ $\mu$ m], and number density of condensation nucleus per unit mass of air  $N/\bar{\rho}$  is  $5.0 \times 10^8$  [kg<sup>-1</sup>] (Tobie et al., 2003).

For space discretization, we use second order centered difference for the terms related to sound wave, and fourth order centered difference for other terms. Time integration is carried out by using time splitting method (Klemp and Wilhelmson, 1978) in which fast modes associated with sound wave and condensation and slow modes are calculated separately. Fast modes are integrated by HE-VI (horizontally explicit and vertically implicit) scheme. We use the Euler scheme as explicit scheme, and Clank-Nicolson scheme as implicit scheme. Slow modes are integrated by leapfrog scheme with Asselin time filter (Asselin, 1972).

Developed numerical models and documents are published in <http://www.gfd-dennou.org/library/deepconv/>.

### 3 Numerical configuration

The computational domain is 50 km in the horizontal direction and 20 km in the vertical direction. Grid spacing is 200 m. Time step is 0.125 or 0.25 sec for fast modes, and 1.0 or 2.0 sec for slow modes. We set surface pressure and temperature to be 7 hPa and 165 K, respectively. We use periodic boundary condition in horizontal direction and stress-free boundary condition in vertical direction. As initial temperature profile, we choose profile in Martian polar cap (Colaprete and Toon, 2002). In this profile, potential temperature is constant (165 K) below 4 km height, and temperature coincides with CO<sub>2</sub> saturation temperature from 4 km height to 15 km height, and temperature is constant (135 K) above 15 km height (Fig.1 left). We determine the initial pressure profile based on hydrostatic equation. As initial perturbation, random noise of potential temperature is added to the lowest layer of atmosphere. We set initial amplitude of heating rate 37.3 K/day below 1 km height, and - 5.0 K/day from 1 km height to 15 km height (Fig.1 right). According to laboratory experiment under the condition of present Martian atmosphere, saturation ratio can rise 1.35 when CO<sub>2</sub> condenses (Glandorf *et al.*, 2002). Therefore we carry out calculations for the case of  $S_{cr} = 1.0$  and 1.35. Integration time are 40 days for the case of  $S_{cr} = 1.0$ , and

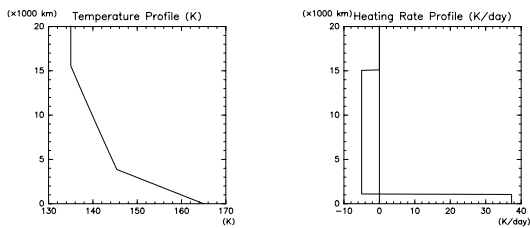


Figure 1: Temperature profile in basic state(left panel) and initial profile of heating rate(right panel).

30 days for the case of  $S_{cr} = 1.35$ .

## 4 Results and discussion

For the case of  $S_{cr} = 1.35$ , quasi-equilibrium state is obtained at about 15th day. In this state, region above 1 km height is covered with clouds (Fig.2). Total cloud mass increases until about 15th day, then becomes nearly constant (Fig.3). Total kinetic energy also becomes nearly constant after 15th day (Fig.4). The deviation field of potential temperature from the zonal mean field is divided into lower layer with 1 km depth and upper layer (Fig.5). While maximum of absolute value of the deviation of potential temperature in lower layer is 2 K, the maximum of absolute value in upper layer is 0.1 K. In lower layer, cooling due to evaporation of clouds are nearly balanced with radiative heating and advection of potential temperature. In upper layer, heating due to condensation and radiative cooling are nearly balanced (figure not shown). Magnitudes of horizontal and vertical component of velocity in lower layer are less than 5 m/s, and these are small compared to those in lower layer (Fig.6, 7). In upper layer, downward flow, though it is weak, exists near  $x = 18 - 32$  [km], and convergent region of cloud are formed on the 30 th day (Fig.2, 7).

In case of  $S_{cr} = 1.0$ , all of cloud evaporates and strong dry convection with one cell occurs. In this case, equilibrium state is not realized on the 40th day. Total cloud mass increases until 2.5th day, then decreases to zero in about 34th day (Fig.8). After complete evaporation of clouds, the deviation of potential temperature and total kinetic energy continue to increase monotonically

(figure not shown). Fig.9, Fig.10 and Fig.11 show the spatial distribution of the deviation of potential temperature, horizontal velocity and vertical velocity after 40 days integration, respectively. One convective cell exist over entire region, and magnitudes values of horizontal and vertical velocity are 145 m/s and 45 m/s, respectively. These values are much larger than those in case of  $S_{cr} = 1.35$ .

The results described above suggest that the difference of critical saturation ratio produces significant difference of structure of moist convection and cloud distribution. In order to investigate the cause for significant difference of convective structure, detailed analysis for structure of the solutions and parameter sweep experiments will be required. Since numerical experiments on terrestrial cloud convection (Nakajima *et al.*, 1998) shows that the falling of condensed matters affects the convective structure, we will also perform calculations with considering the falling of condensed matters.

## Acknowledgement

Figures are plotted by the use of the softwares developed by Dennou Ruby Project (<http://ruby.gfd-dennou.org/>). Numerical calculations are performed by the NEC SX9 of the ISAS/PLAIN Center, JAXA.

## References

- Asselin, R., 1972: "Frequency filter for time integrations", *Mon. Wea. Rev.*, 100, 487 – 490.
- Colaprete, A., Toon, O. B., 2002: "Carbon dioxide snow storms during the polar night on Mars", *J. Geophys. Res.*, 107, 5051, doi:10.1029/2001JE001758.
- Colaprete, A., Haberle, R. M., Toon, O. B., 2003: "Formation of convective carbon dioxide clouds near the south pole of Mars. " *J. Geophys. Res.* 108(E7), 5081, doi:10.1029/2003JE002053
- Forget, F., Pierrehumbert, R. T., 1997: "Warming early Mars with carbon dioxide clouds that scatter infrared radiation", *Science*, 278, 1273 – 1276.
- Glandorf, D. L., Colaprete, A., Tolbert, M. A., Toon, O. B., 2002: "CO<sub>2</sub> snow on Mars and early Earth: experimental constraints", *Icarus*, 160, 66 – 72.

Klemp, J. B., Wilhelmson, R. B., 1978: “The simulation of three-dimensional convective storm dynamics”, J. Atmos. Sci., 35, pp. 1070 – 1096.

Mitsuda, C., 2007: “The greenhouse effect of radiatively adjusted CO<sub>2</sub> ice cloud in a Martian paleoatmosphere”(in Japanese), Doctoral thesis of Division of Earth and Planetary Sciences, Graduate School of Science, 115 pp.

Nakajima, K., Takehiro, S., Ishiwatari, M., Hayashi, Y.-Y., “Cloud convections in geophysical and planetary fluids”(in Japanese), Nagare Multimedia, <http://www2.nagare.or.jp/mm/98/nakajima/index.htm> (1998).

Nakajima, K., Takehiro, S., Ishiwatari, M., Hayashi, Y.-Y., 2000: “Numerical modeling of Jupiter’s moist convection layer”, Geophys. Res. Lett., 27, 3129–3132.

National Astronomical Observatory of Japan, 2004: “Chronological scientific tables ” (in Japanese), Maruzen, 1015 pp.

Odaka, M., Kitamori, T., Sugiyama, K., Nakajima, K., Hayashi, Y.-Y., 2006: “A numerical simulation of Martian atmospheric moist convection”(in Japanese), Proceeding of the 20 th ISAS Atmospheric Science Symposium, 103 – 106.

Pettengill, G. H., Ford, P. G., 2000: “Winter clouds over the north Martian polar cap”, Geophysical Research Letters, 27, 609 – 612.

Sugiyama, K., Odaka, M., Nakajima, K., Hayashi, Y.-Y., 2009: “Development of a cloud convection model to investigate the Jupiter’s atmosphere”, Nagare Multimedia, <http://www2.nagare.or.jp/mm/2009/sugiyama/index.htm>

The society of chemical engineers of Japan, 1999: “The handbook of chemistry and engineering”(in Japanese), Maruzen, 1339 pp.

Tobie, G., Forget, F., Lott, F., 2003: “Numerical simulation of winter polar wave clouds observed by Mars Global Surveyor Mars Orbiter Laser Altimeter”, Icarus, 35, 33 – 49.

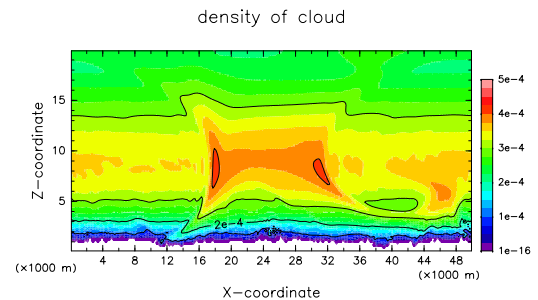


Figure 2: A snapshot for distribution of cloud density at 30 day in case of  $S_{cr} = 1.35$  without falling of cloud particle.

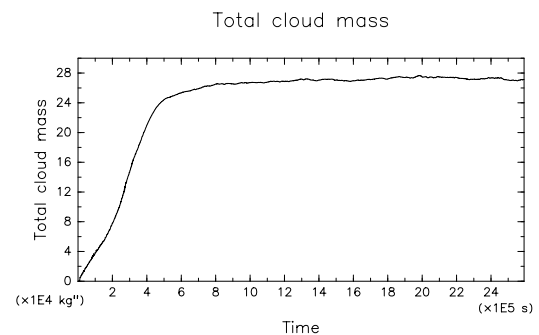


Figure 3: Time evolution of total cloud mass from 0 day to 30 day in case of  $S_{cr} = 1.35$  without falling of cloud particle.

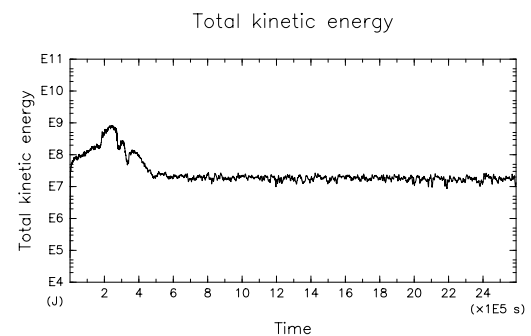


Figure 4: Time evolution of total kinetic energy from 0 day to 30 day in case of  $S_{cr} = 1.35$  without falling of cloud particle.

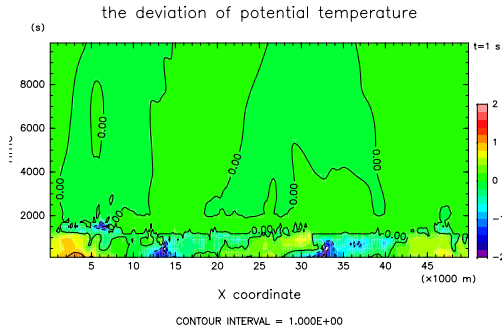


Figure 5: Same as in Fig.2 but for the deviation of potential temperature from the zonal mean field. Vertical range from 0 km to 10 km is shown.

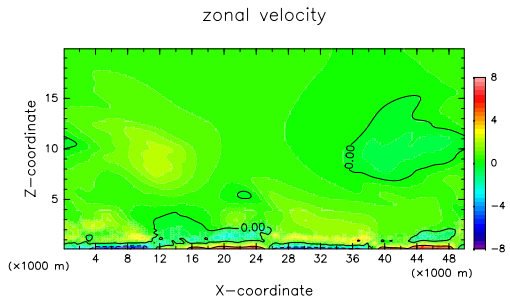


Figure 6: Same as in Fig.2 but for horizontal velocity.

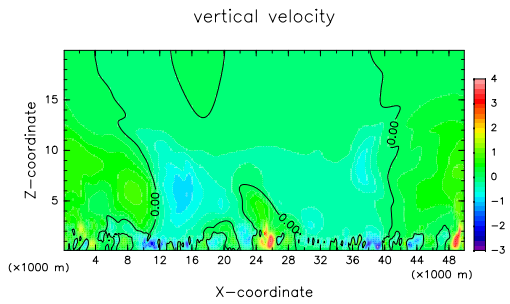


Figure 7: Same as in Fig.2 but for vertical velocity.

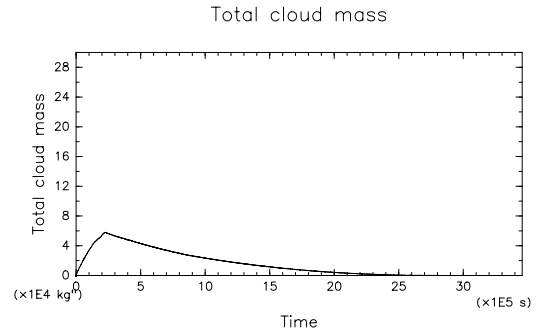


Figure 8: Time evolution of total cloud mass from 0 day to 40 day in case of  $S_{cr} = 1.0$  without falling of cloud particle.

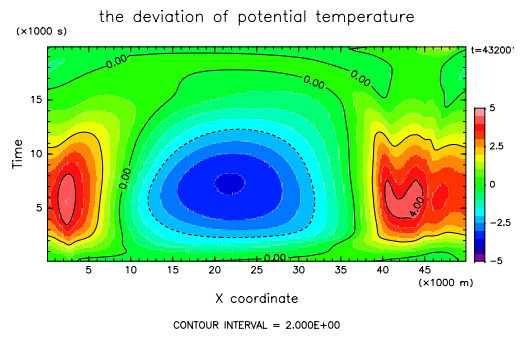


Figure 9: A snapshot for distribution of the deviation of potential temperature from the zonal mean field at 40 day in case of  $S_{cr} = 1.0$  without falling of cloud particle.

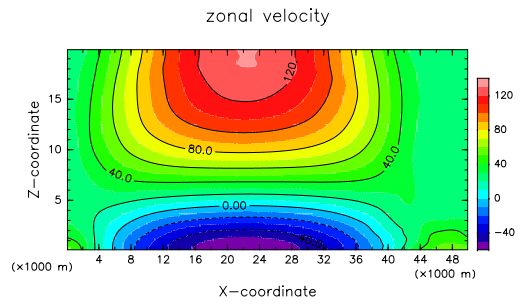


Figure 10: Same as in Fig.9 but for horizontal velocity.

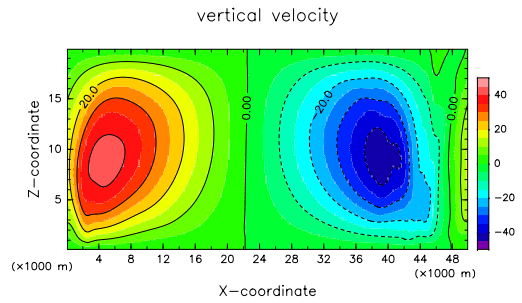


Figure 11: Same as in Fig.9 but for vertical velocity.